9-21-2017

Altering the Coordination of Iron Porphyrins by Ionic Liquid Nanodomains in Mixed Solvent Systems

Abderrahman Atifi
Marquette University

Michael D. Ryan
Marquette University, michael.ryan@marquette.edu

Accepted version. *Chemistry- A European Journal*, Vol. 23, No. 53 (September 21, 2017): 13076-13086. DOI.

Chemistry-A European Journal, Vol. 23, No. 53 (September, 2017): 13076-13086. DOI.

Contents

Altering the Coordination of Iron Porphyrins by Ionic Liquid Nanodomains in Mixed Solvent Systems

Abderrahman Atifi
Marquette University, Milwaukee, WI
Michael D. Ryan
Marquette University, Milwaukee, WI

Abstract

The solvent environment around iron porphyrin complexes was examined using mixed molecular/RTIL (room temperature ionic liquid) solutions. The formation of nanodomains in these solutions provides different solvation environments for substrates that could have significant impact on their chemical reactivity. Iron porphyrins (Fe(P)), whose properties are sensitive to solvent and ligation changes, were used to probe the molecular/RTIL environment. The addition of RTILs to molecular solvents shifted the redox potentials to more positive values. When there was no ligation change upon reduction, the shift in the *E*° values were correlated to the Gutmann acceptor number, as was observed for other porphyrins with similar charge changes. As %RTIL approached 100%, there was insufficient THF to maintain coordination and the *E*° values were much more dependent upon the %RTIL. In the case of $Fe^{III}(P)(Cl)$, the shifts in the *E*° values were driven by the release of the chloride ion and its strong attraction to the ionic liquid environment. The spectroscopic properties and distribution of the Fe^{II} and Fe^{I} species into the RTIL nanodomains were monitored with visible spectroelectrochemistry, ^{19}F NMR and EPR spectroscopy. This investigation shows that coordination and charge delocalization (metal versus ligand) in the metalloporphyrins redox products can be altered by the RTIL fraction in the solvent system, allowing an easy tuning of their chemical reactivity.

Introduction

Room temperature ionic liquids (RTILs) have been shown to be efficient catalysts for the activation of small molecules such as CO_2. Their ionic structure can bypass the single electron reduced intermediate, which is often energetically unfavorable. On the other hand, RTILs are expensive and have high viscosities which may limit their application. To minimize these effects, they are often mixed with

molecular solvents. It will be the aim of this work to probe the relationship between bulk properties of the molecular solvent/RTIL mixtures with the physical properties of the solutes (such as visible spectra and redox potentials) as the ratio of molecular solvent to RTIL changes. While there have been many reports on the relationship between the solute's physical properties and the bulk properties of RTILs[1] and relating them to molecular solvents, there have been fewer studies on mixed molecular solvent/RTIL mixtures.[2] Changes in these molecular properties can give a unique insight into the interaction between solutes and mixed molecular solvent/RTIL solutions.[2c]

Metal catalysts such as metalloporphyrins are often able to activate small molecules such as CO_2, O_2, NH_3, and N_2. For example, Savéant et al.[3] showed that it was feasible to convert CO_2 to CO with low valent iron porphyrins. Significantly larger efficiencies were obtained using proton sources as part of the catalyst.[4] Metals other than iron have also been used as a CO_2-reduction catalyst.[5] Alternatively, RTILs can be used to lower the energy for the electron transfer by ion pairing with the charged species that are formed. This approach was used by Rosen et al.,[6] along with a proton source and a silver electrode to greatly reduce the overpotential for the CO_2 to CO conversion. Both approaches were combined by Choi et al.[7] In their work, an iron porphyrin/RTIL co-catalyst and a proton donor were used to increase the CO_2 to CO reduction efficiency. In order to develop the best catalyst, the influence of all these factors need to be understood. Although most of the focus has been on CO_2 activation, RTILs have used in the activation of other small molecules. The reduction of N_2 to ammonia occurred much more efficiently at an RTIL-coated working electrode.[8] The addition of RTILs has also been found to increase the efficiency of the oxygen reduction reaction (ORR),[9] as well as the oxidation of ammonia to dinitrogen.[10] An understanding of the interactions between the RTIL and the CO_2-reducing catalyst can have a significant impact on the reduction product. Lau et al.[11] examined the role of an imidazolium based RTIL on the reduction of CO_2 at a silver electrode. The role of the RTIL is involved not only in the efficiency of CO_2 reduction, but also with the identity of the ultimate product.[12] Sun et al.[13] examined the role of RTILs in switching the reduction product from oxalate to CO. The reduction of CO_2 in molecular solvents has been studied extensively using voltammetry,[14] or by DFT methods.[5b] When RTILs are mixed with molecular solvents, the ions are only homogeneously dispersed at low concentrations.[15] At higher concentrations, nanodomains of RTILs are formed,[16] with initially islands of RTIL in a molecular solvent matrix (solvent-rich mixture) to eventually molecular solvent islands in a RTIL matrix (RTIL-rich mixture). Substrates can partition between these two nanodomains (molecular solvent/RTIL), and, in these nanodomains, sense an environment that differs from the bulk parameters. The extent of this partitioning can have a significant effect on the redox potentials, especially for dianions (e.g., DNB^{2-}, DNB=dinitrobenzene)[2d, 17] or monoanions that interact strongly with the RTIL ($NiOEPone^-$, OEPone=octaethylporphinone).[2e] For example, the two one-electron waves of dinitrobenzene can collapse into a single two-electron wave in an ionic liquid.[2d, 17] Nikitina et al.[18] showed significant shifts in the $E°$ values, especially for dianionic species. In addition, planar species are more likely to partition in the RTIL nanodomain than spherical substrates.[2f] The solution structure of redox catalysts in the presence of RTILs has a significant effect on their redox potential and their ability to interact with substrates. It has been shown that this interaction can extend beyond the stabilization of the anionic species, and can lead to changes in the electronic structure of the species.[2e] For example in $Ni(OEPone)^-$, the infrared band for the carbonyl band was significantly downshifted in the presence of the RTIL, and the visible spectrum of this species showed significant differences in the Soret band as compared to the spectrum in molecular solvents. The $Ni(OEPone)^-$ spectrum in RTILs was most similar to a Ni^{II} porphyrin

radical anion as opposed to a Ni^{I} species in molecular solvents. The changes in the infrared and visible spectra were attributed to the strong interactions between the porphyrin anion and the RTIL.

In the examples above, the changes that we observed in the presence of the RTIL were mainly the effect of solvation due to ion pairing or nanodomains. Changes in the molecular structure due to coordination changes were not studied. Iron porphyrins, a common redox catalyst, can form complexes with a coordination number of 4–6 in solution, as well as changes in the spin state and oxidation state. Therefore, the presence of RTILs in mixed molecular solvent/RTIL solution can change the redox behavior of the iron catalyst by changing ligation solvation or spin-state of the complex. Changes in coordination have a significant effect on the catalytic properties of these complexes, especially in regards to substrate bonding. In this report, we will examine the effect of RTILs in mixed solutions on the redox properties, coordination number and electronic state of iron porphyrins in order to understand the interaction between the solute and the molecular solvent/RTIL system.

Results and Discussion

Cyclic Voltammetry of Fe(FP)(ClO_4)/Cl in pure solvents

The effect of RTILs on iron porphyrin redox properties was first examined using cyclic voltammetry. In order to maximize the solubility of the ferric porphyrin in the RTIL solution, the tetra(pentafluorophenyl)porphyrin (FP) ligand was used in this work. In addition, the presence of fluorine atoms on the phenyl groups significantly lowered the redox potential of each step, and had the added advantage that ^{19}F NMR could be exploited to investigate the effect of RTILs on the different redox states of the iron porphyrin. Ferric porphyrin can be reduced in three one electron redox processes as shown below (omitting ligand/solvent coordination [Eq. 1-3]:

$$Fe^{III}(FP)^{+}e^{-} \rightarrow Fe^{II}(FP) \quad (1)$$

$$Fe^{II}(FP) + e^{-} \rightarrow Fe^{I}(FP)^{-} \quad (2)$$

$$Fe^{I}(FP)^{-} + e^{-} \rightarrow Fe^{0}(FP)^{2-} \quad (3)$$

In THF, the perchlorate ligand in Fe(FP)(ClO_4) was displaced by the THF solvent to form the bis-THF complex.[19] The three reduction waves in THF are shown in Figure 1 (red trace). In order to minimize the changes in the potential as the solvent system was changed, all potentials (Table S1) were referenced versus decamethylferrocene (DmFc).[20] In $AmNTf_2$ (ethyldimethylpropylammonium bis(trifluoromethylsulfonyl)imide), only two reversible waves were observed. Both waves were shifted to more positive potentials (Figure 1, blue trace), with the second wave being shifted more strongly than the first. As expected from the increased viscosity of $AmNTf_2$ versus THF, the current was significantly lower in $AmNTf_2$, but was consistent with the Stokes–Einstein equation. The third wave, which was observed in THF, was not observed in $AmNTf_2$ due to the narrowing of the solvent window. This was not an intrinsic property of $AmNTf_2$ as a wider window was observed for other substrates. The failure to observed this wave was probably due to the reaction of $Fe(P)^{2-}$ with tetraalkylammonium ions.[21] The shift in the $E°_1$ between THF and $AmNTf_2$ was 167 mV, while the $E°_2$ potential shifted by 322 mV, nearly twice as much. In both solvents, the first and second redox processes were nearly reversible. Including solvent coordination, the first wave in THF for Fe(FP)(ClO_4) can be written as Eq. 4:

$$Fe^{III}(FP)(THF)_2^+ + e^- \rightleftarrows Fe^{II}(FP)(THF)_2 \text{ (4)}$$

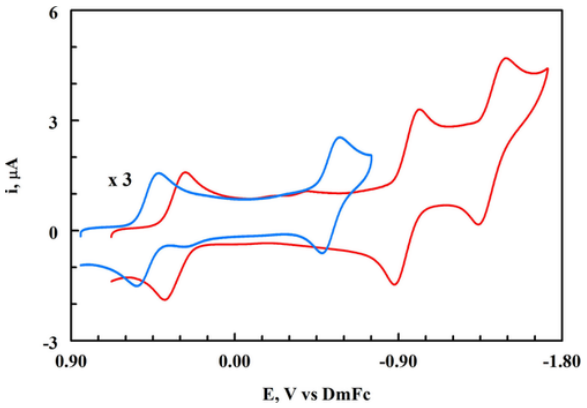

Figure 1 Cyclic voltammetry of 0.6 mM Fe(FP)(ClO_4) in THF (red trace) and in $AmNTf_2$ (blue trace, current multiplied by a factor of 3). Scan rate: 100 mV s^{-1}. Potential referenced vs. decamethylferrocene (DmFc).

Previous work has shown that the ferrous complex is also a bis-THF complex.[22] In $AmNTf_2$, the coordination of the ferric complex is unclear as perchlorate and NTf_2^- are both conjugate bases of superacids with similar pK_a values for their conjugate acids.[23] Based on the pK_a values in dichloroethane, perchlorate is a weaker base than NTf_2^- though the latter species might not bind as well due to steric reasons. On the other hand, the large concentration difference between ClO_4^- and NTf_2^- would favor coordination by the latter. The reversibility of the both reductions in $AmNTf_2$, though, are consistent with the absence of coordination changes upon reduction. The solvent coordination of the ferrous species will be examined in more detail using spectroscopic methods. The shift in the $E°_1$ and $E°_2$ values in changing the solvent from THF to $AmNTf_2$ was larger than was observed for $Ni(OEP)^{+/0}$ (101 mV) and $Ni(OEP)^{0/-1}$ (234 mV) where the charge changes are the same as for the first and second reductions of Fe(FP)(ClO_4). The cyclic voltammetric results indicate a very strong stabilization of the reduced species by the RTIL.

In Figure 2, the cyclic voltammetry in THF of Fe(FP)Cl (green trace) is compared to the voltammetry of Fe(FP)(ClO_4) (red trace). The first reduction of Fe(FP)(Cl) in THF was shifted to more negative potentials as compared to Fe(FP)(ClO_4) (261 mV). This large shift was due to chloride ligation of the Fe(FP)(Cl) species. The first wave can be written as [Eq. 5]:

$$Fe(FP)(Cl) + e^- + 2THF \rightarrow Fe(FP)(THF)_2 + Cl^- \text{ (5)}$$

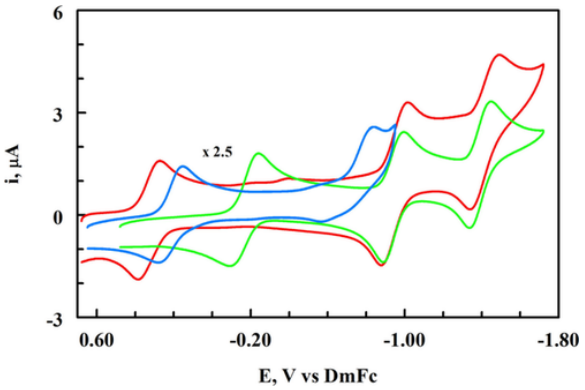

Figure 2 Cyclic voltammetry of 0.6 mM $Fe(FP)(ClO_4)/Cl$ in THF and $AmNTf_2$ at 100 mV s^{-1}. $Fe(FP)(ClO_4)$ in THF: red trace; Fe(FP)Cl in THF: green trace; Fe(FP)Cl in $AmNTf_2$: blue trace (current multiplied by 2.5). Potential referenced vs. decamethylferrocene (DmFc).

The peak potentials for the second wave in THF for $Fe(FP)(ClO_4)$ and Fe(FP)(Cl) occurred at nearly the same potential (−1.016 V), indicating that the same redox process occurred in THF (Reaction 2). This result also confirmed the loss of Cl^- from the complex upon the ferric reduction. Otherwise, the second wave would have been shifted to a potential negative of the $Fe(FP)(ClO_4)$ complex.

The cyclic voltammetry of Fe(FP)(Cl) in $AmNTf_2$ is shown in Figure 2 (blue trace). The first wave was shifted positive of the wave in THF (382 mV). This was a considerably larger shift that was observed for $Fe(FP)(ClO_4)$ (167 mV). The second wave was not shifted as much and was not reversible. In this case the ΔE_p value will be used instead of the $\Delta E°$ value. The difference in peak potentials between the second wave in THF and in $AmNTf_2$ was 156 mV. More importantly, the second peak potential of Fe(FP)(Cl) in $AmNTf_2$ was 262 mV negative of the wave for $Fe(FP)(ClO_4)$, in that same solvent. This indicates that the redox couple for Fe(FP)(Cl) was different from that of $Fe(FP)(ClO_4)$ in $AmNTf_2$. This will be investigated more later, but, at this point, the evidence indicates that the ferrous complex remained coordinated to chloride on the voltammetric timescale [Eq. 6–8].

$$Fe^{III}(FP)(Cl) + e^- \rightleftarrows Fe^{II}(FP)(Cl^-) \quad (6)$$

As a result, the second wave involved both the reduction of iron and the loss of chloride, leading to an irreversible wave (EC mechanism).

$$Fe^{II}(FP)(Cl)^- + e^- \rightleftarrows Fe(FP)(Cl)^{2-} \quad (7)$$

$$Fe(FP)(Cl)^{2-} \rightleftarrows Fe(FP)^- + Cl \quad (8)$$

For the second reduction, there is no net change in the charge of the metal complex so its solvation in the RTIL should be similar. From an energetics point of view, the solvation of Cl^- by the RTIL could be responsible for the positive shift in the redox potential. Spectroscopic studies that will be discussed later will investigated the coordination structure of the reduction products.

Visible spectroelectrochemistry of $Fe(FP)(ClO_4)/Cl$ in pure solvents

The visible spectroelectrochemistry of $Fe(FP)(ClO_4)$ in THF is shown in Supporting Information Figure S1 (red trace). The results are summarized in Table 1. The spectra of $Fe(FP)^+$, Fe(FP), and $Fe(FP)^-$ are similar to their tetraphenylporphyrin (TPP) analogues, with small blue shifts in the Soret band for the FP

complexes. In THF, the Soret band for $Fe(FP)^-$ was more bleached than the $Fe(TPP)^-$ complex.[24a,24c] The spectroelectrochemistry of $Fe(FP)(ClO_4)$ in $AmNTf_2$ is shown in Figure 3. The spectrum of the ferric complex in $AmNTf_2$ was quite similar to the complex in THF, with only a slight blueshift in the Soret band (THF: 394 nm; $AmNTf_2$: 392 nm). The ferric complex in THF has been identified as a bis-THF adduct. As NTf_2^- has a basicity very similar to ClO_4^-, the large concentration difference would favor NTf_2^- coordination. The Soret band for the ferrous complex (first reduction product) in $AmNTf_2$ (410 nm) was blue-shifted from the band in THF (420 nm), but otherwise the spectra appeared to be similar. The ferrous complex in THF is known to be a bis-THF complex, as was the ferric complex. The visible spectra of 4-, 5- and 6-coordinate ferrous porphyrins complexes are well known. A 4-coordinate complex such as Fe(TPP) in benzene or dichloromethane has a split Soret band with peaks at 420 and 455 nm.[25] For 5-coordinate anions complexes such as halide complexes of Fe(TPP), the Soret band is redshifted (440 nm).[26] While one might expect such a spectrum for Fe(FP) in $AmNTf_2$, NTf_2^- is a very weak ligand, and the charge is quite diffuse. Formally, the negative charge is on the nitrogen atom (NTf_2^-: $F_3C\text{-}SO_2\text{-}N\text{-}SO_2\text{-}CF_3^-$). This atom can ion pair with the solvent cation, leaving the relatively neutral SO_2 group to interact with the iron atom. A bis-coordination is possible with this structure. As a result, the interaction of the SO_2 group with the iron atom is more like a weak solvation interaction, rather than a covalent iron–anion bond. The coordination of the ferric/ferrous complexes with NTf_2^- will be examined later by ^{19}F NMR.

Table 1. UV/Visible spectra of various iron porphyrin complexes

Compound	Solvent	Soret	Other bands	Reference
$Fe(FP)(ClO_4)$	THF	394	504	this work
	$AmNTf_2$	392	510, 600	this work
Fe(FP)(Cl)	THF	400	–	this work
	$AmNTf_2$	408	498	this work
Fe(FP)	THF	420	540	this work
	$AmNTf_2$	410	558	this work
$Fe(FP)^-$	THF	410 (broad)		this work
	$AmNTf_2$	434	556, 620	this work
$Fe(FP)^{2-}$	THF	350, 454	526	this work
$Fe(TPP)(ClO_4)$	THF	400	526, 658	[24a]
	CH_2Cl_2	380	500, 633	[24b]
Fe(TPP)	THF	424	536, 601	[24c]
	DMF	434	562	[24d]
	dichloroethane	417	443, 537	[24e]
$Fe(TPP)^-$	THF	392, 424	512, 576s, 605s, 674	[24c]
$Fe(TPP)^{2-}$	THF	360, 424, 460	580,608	[24c]
	DMF	362, 460	526, 556	[24f]

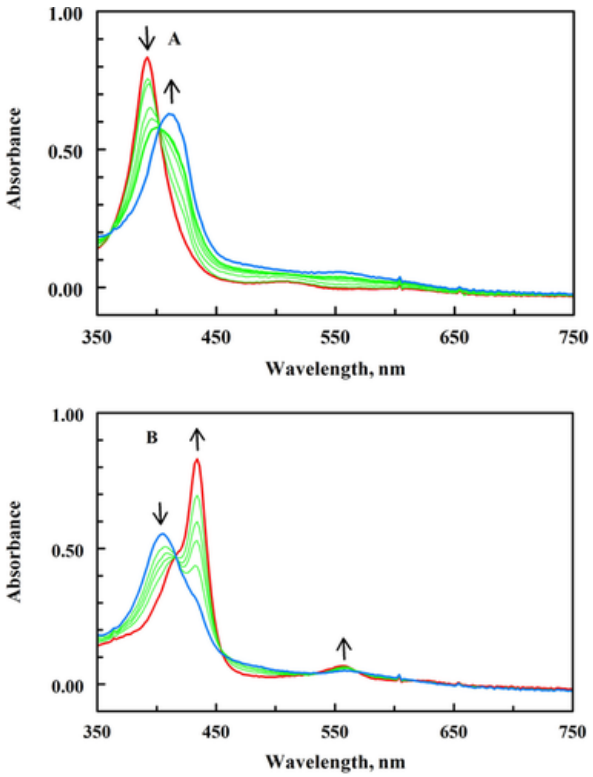

Figure 3 Visible spectroelectrochemistry of 0.5 mm Fe(FP)(ClO_4) in $AmNTf_2$. A) First reduction at −0.60 V vs. Ag/$AgNO_3$. Red: 0 s; Green: 10, 45, 90, 110, 130 s; Blue: $Fe(FP)^-$. B) Second reduction at −1.20 V vs. Ag/$AgNO_3$. Blue: 0 s; Green: 10, 20, 30, 50 s; Red: 200 s.

The second reduction of Fe(FP)(ClO_4) in $AmNTf_2$ (Figure 3 B) yielded a spectrum that was considerably different from the spectrum in THF (Figure S1B). The Soret band for $Fe^{I}(FP)^-$ was almost completely bleached in THF, but a strong Soret band was observed in $AmNTf_2$, with an absorbance maximum at 434 nm. The stronger Soret band may indicate less delocalization of the Fe^{I} electron density to the porphyrin ring in $AmNTf_2$.

In the spectroelectrochemical reduction of Fe(FP)(Cl) in THF (Figure S2), the same ferrous complex was formed as was observed with Fe(FP)(ClO_4), indicating that the first reduction product was a bis-THF ferrous porphyrin. Similarly, the products of the second and third reduction of Fe(FP)(Cl) was the same as were observed with Fe(FP)(ClO_4) (Figure S2).

The spectra in $AmNTf_2$ were considerably more complex than were observed for the perchlorate complex because of the ability of Cl^- to coordinate with Fe^{II}. At higher concentrations of the ferric porphyrin, the reduction of Fe(FP)Cl in $AmNTf_2$ gave clear isosbestic points over the entire reduction, but yielded a spectrum significantly different from that observed in THF. The ferrous spectrum was consistent with a $Fe(FP)Cl^-$ complex with a Soret band at 435 nm (Figure 4 A), considerably shifted from the 410 nm Soret band for the perchlorate complex. If the spectroelectrochemistry was carried out at lower concentrations of ferric porphyrin, significant dissociation of $Fe(FP)(Cl)^-$ occurred, and the band at 414 nm was observed, similar to the $Fe^{II}(FP)$ spectrum in $AmNTf_2$ generated from Fe(FP)(ClO_4). This confirms the tentative assignment of the initial products in Reaction 6. While $Fe(FP)(Cl)^-$ is the initial ferrous complex, a slow dissociation of Cl^- does occur (Figure 4 B), forming the $Fe^{II}(FP)$ complex which

was very similar to the ferrous complex in THF. While the slow dissociation is quite important for spectroscopic studies, the voltammetric results will reflect a chloride coordinated ferrous complex.

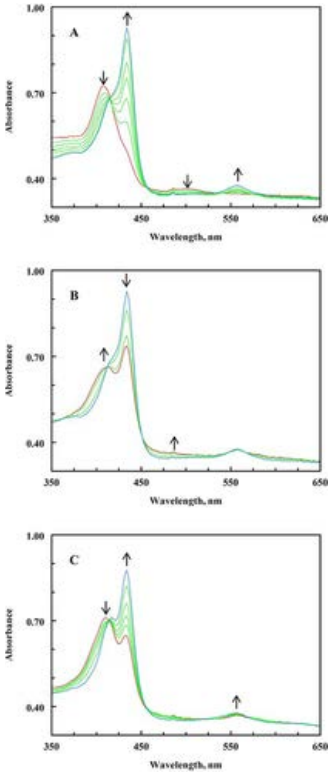

Figure 4 Visible spectroelectrochemistry of 0.5 mm Fe(FP)(Cl) in $AmNTf_2$. A) First reduction. $E_{applied}$=−0.60 V vs. $Ag/AgNO_3$. Red: 0 s; Green: 50, 500, 1000, 1500, 2500 s; Blue: 4000 s. B) First reduction. $E_{applied}$=−0.60 V vs. $Ag/AgNO_3$. Blue: 4000 s; Green: 5957 s, 7960 s; Red: 9262 s. C) Second Reduction. $E_{applied}$=−1.40 V vs. $Ag/AgNO_3$. Red: 63 s; Green: 313, 463, 713, 1214 s. Blue: 3467 s. All times are measured from the beginning of the potential step.

When the potential was stepped to the second wave (Figure 4 C), the spectrum in $AmNTf_2$ was consistent with the $Fe(FP)^-$ complex formed from $Fe(FP)(ClO_4)$. This indicated that the same spectral species was formed in $AmNTf_2$, whether one started with Fe(FP)(Cl) or $Fe(FP)(ClO_4)$. While the transition from Fe(FP) to $Fe(FP)^-$ in $AmNTf_2$ is clear in this experiment, a comparison of the blue traces in Figure 4 A ($Fe(FP)(Cl)^-$) and in Figure 4 C ($Fe(FP)^-$) show the spectra are quite similar (Figure S3). The Soret bands differ by about 2 nm ($Fe(FP)^-$: 433 nm; $Fe(FP)(Cl)^-$: 435 nm), and the Q-band for $Fe(FP)^-$ was 557 nm, while it was 566 nm for $Fe(FP)(Cl)^-$. If the scan rate was increased or the step time was decreased, the conversion of $Fe(FP)(Cl)^-$ to Fe(FP) will not occur, and the spectral changes upon reduction were not as large as was observed in Figure 4. Further spectroscopic studies using NMR and EPR will provide additional confirmation that the species are indeed different, but the results from Figure 4 clearly show that the conversion from Fe(FP) to $Fe(FP)^-$ will only occur at a more negative potential.

In the reverse scan, at −0.60 V vs. $Ag/AgNO_3$, the band for $Fe^{II}(FP)$ appeared first, and then followed by the formation of some $Fe^{II}(FP)(Cl)^-$ species, though the chloride complex is still a minor species. Further oxidation at +0.40 V ultimately led to the formation of Fe(FP)(Cl) (Figure S4).

Cyclic voltammetry of Fe(FP)(ClO_4)/Cl in mixed RTIL/molecular solvents

The voltammetric and spectroscopic studies in THF and $AmNTf_2$ have shown significant differences for the iron complexes between the molecular and RTIL environment. Previous work has shown the formation of nanodomains in mixed solvent which will preferentially solvate solutes in the mixture.[2e,27] In order to investigate the effect of these nanodomains on substrates, the voltammetry of Fe(FP)(Cl)/(ClO_4) was investigated in mixed solvent solutions. In Figure 5 A (red symbols), the variation in the $E°_1$ values vs. DmFc for Fe(FP)(ClO_4) as a function of log(%RTIL) is shown. For most of the mixture ratios, the $E°_1$ values for Fe(FP)(ClO_4) were linearly dependent upon the log(%RTIL) until the solution became nearly pure $AmNTf_2$. At 100 % $AmNTf_2$, there was a significant discontinuity.

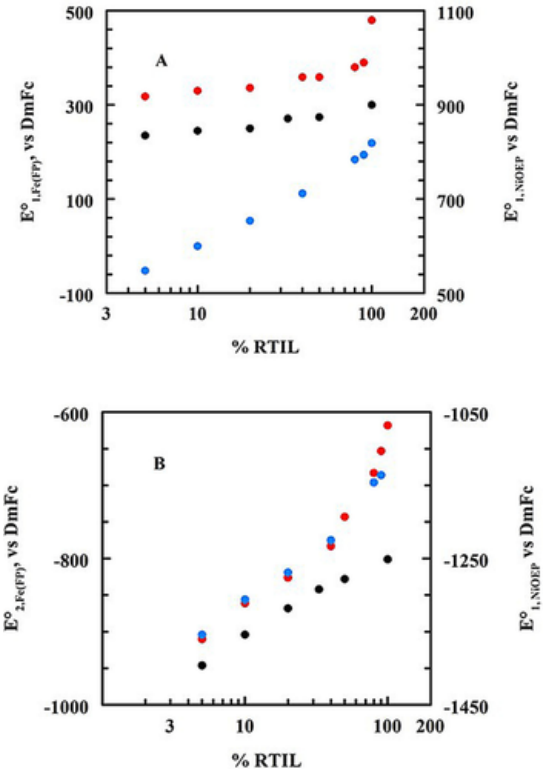

Figure 5 Variation of the $E°$ values in THF/$AmNTf_2$ mixtures as a function of the %RTIL. A) $E°_1$ for Fe(FP)(ClO_4)/(Cl) and $E°$ for the oxidation of Ni(OEP). B) $E°_2$ for Fe(FP)(ClO_4)/(Cl) and $E°$ for the reduction of Ni(OEP). Compound: Fe(FP)(ClO_4) (λ), left axis; Fe(FP)(Cl) (λ), left axis; Ni(OEP) (λ), right axis.

In THF, the first redox process is given by Reaction 4. This involved the transformation from a cation to a neutral species. For comparison, the variation in the $E°$ values for Ni(OEP) oxidation is also shown in Figure 5 A (black symbols). As can be seen, the slope of these two curves are quite similar until the solutions approach 100 % RTIL. At this point, there is significant curvature in the $Fe(FP)^+$/Fe(FP) process, but not in the $Ni(OEP)^+$/Ni(OEP) reduction. Plotting the same data versus the Gutmann acceptor number (AN) (Figure S5A), the transition towards 100 % RTIL is more pronounced. In this plot, a modest curvature is seen for Ni(OEP) while a more pronounced trend is seen for $Fe(FP)^+$. Clearly, the loss of THF coordination affected the $Fe(FP)^+$/Fe(FP) potential more than the $Ni(OEP)^+$/Ni(OEP) potential. The variation in Fe(FP)(Cl)/Fe(FP) redox potential as a function of the Gutmann AN is also plotted in Figure S5 (green symbols). In this case, the redox process is given by Reaction 5. The porphyrin species is

uncharged in both the ferric and ferrous states but the net change is from neutral to negative one. RTILs generally affect the 0/-1 transition more than the +1/0 transition, and this was the case here. The steep slope for the *E*° value for Fe(FP)(Cl) versus %RTIL and Gutman AN is consistent with the stronger solvation of anions. Figure 5 B shows the slope of the *E*° for Ni(OEP)/Ni(OEP)$^-$ as a function of log(%RTIL), which is comparable to the variation of the *E*° for Fe(FP)(Cl)/Fe(FP) in Figure 5 A. Because the charge on the ferric and ferrous porphyrins are the same (neutral), the solvation of these species should be similar in $AmNTf_2$, but the Cl^- would be strongly solvated in the RTIL nanodomain. The strong solvation of this ion drives the *E*° to more positive potentials, rather than the solvation of the porphyrin species in the RTIL nanodomain (as was observed for Ni(OEPone)).[2e] The strong nonlinearity for the *E*° values for $Fe(FP)^+$/Fe(FP) occurred as the ligand THF for the ferric and ferrous species were replaced with NTf_2^-. This behavior was unusual compared to other redox species that have been previously examined. Previous work with Ni(OEP),[2e] C_{60}[2f] and dinitrobenzene[2d] showed that there was significant linearity over the entire log(%RTIL) range. This would indicate a significant change in the solvation environment when the mixtures reflect primarily the RTIL nanodomain.

For the second reduction, the *E*° values for the $Fe(FP)(ClO_4)$ and Fe(FP)(Cl) complexes were strongly dependent upon the %RTIL (Figure 5 B). For both species, the charge transition was from 0 to −1. There was little difference between the chloro- and perchlorate-complexes of Fe(FP) as the %RTIL changed. The slopes were similar to the Ni(OEP)$^{0/-}$ redox process (Figure 5 B). The non-linearity of the $E°_2$ values started at a much lower %RTIL (about 70 %), with significantly larger stabilization of the reduced species. This change in slope was not observed for the Ni(OEP)$^{0/-}$ reduction at higher %RTIL. Clearly, as the %RTIL increased, the solvation/coordination environment changed significantly.

As was discussed in the previous section, the voltammetry of Fe(FP)(Cl) had an anomaly that the second reduction was less reversible in $AmNTf_2$ than in THF. Interestingly, when a small amount of THF was added, the reversibility of the $Fe^{II}(FP)$/$Fe(FP)^-$ wave improved considerably (Figure S6). The shape of the wave was consistent with the dissociation of chloride from the $Fe(FP)(Cl)^-$ complex, rather than a quasi-reversible electron transfer or uncompensated resistance (the first wave in the voltammogram reflects uncompensated resistance). These results are consistent with Reactions 7–8.

Visible spectroelectrochemistry of $Fe(FP)(ClO_4)$/Cl in mixed RTIL/molecular solvents

The visible spectroelectrochemistry of $Fe(FP)(ClO_4)$ has shown that $Fe^{II}(FP)$ and $Fe(FP)^-$ have distinctive spectra in the THF and $AmNTf_2$ environment especially in the Soret region. In order to interpret the voltammetric data in mixed solvents, the visible spectroelectrochemistry of $Fe(FP)(ClO_4)$ was undertaken. This is the simpler complex to interpret because the ferric and ferrous species are solvent coordinated in THF. From the features of the visible spectrum it should be possible to interpret the solvent environment around the iron species in mixed THF/RTIL solutions.

The first reduction of $Fe(FP)(ClO_4)$ in 50 % THF/$AmNTf_2$ is shown in Figure 6 A. The spectra are qualitatively similar to the reduction in THF. The Soret band shifted from 392 to 418 nm upon reduction. A close examination of Figure 6 A, though, shows a smaller Soret band at about 410 nm which is the λ_{max} for $Fe^{II}(FP)$ in $AmNTf_2$. Figure 6 B shows the visible spectra for $Fe^{II}(FP)$ in 50 % THF/$AmNTf_2$, THF and $AmNTf_2$. It is clear that the ferrous species has partitioned between the two nanodomains. While the $Fe^{II}(FP)$ band for the THF nanodomain dominates, the $Fe^{II}(FP)$ Soret band in $AmNTf_2$ is weaker so an overall analysis shows that $Fe^{II}(FP)$ roughly equally distributed between the THF and RTIL nanodomains.

The stronger solvation by the $AmNTf_2$ nanodomain would shift the $E°_1$ values positively as the $\%AmNTf_2$ is increased.

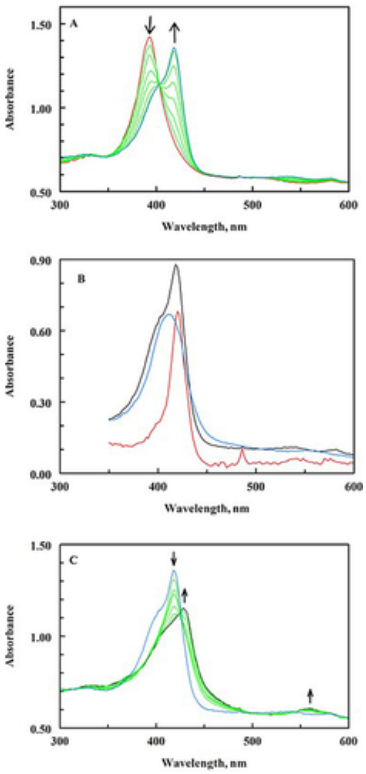

Figure 6 Visible spectroelectrochemistry of 0.5 mm $Fe(FP)(ClO_4)$ in THF/50 $\%AmNTf_2$. A) First reduction. Red: +0.20 V; Green: −0.02, −0.06, −0.10, −0.14, −0.20, −0.28 V. Blue: −0.32 V. B) Black trace: $Fe^{II}(FP)$ in 50 % THF/$AmNTf_2$; red trace: $Fe^{II}(FP)$ in THF; blue trace: $Fe^{II}(F)$ in $AmNTf_2$. C) Second reduction. Blue: −0.32 V; Green: −0.72, −0.82, −0.88, −0.94, −0.98 V; Black: −1.00 V. All potentials vs. $Ag/AgNO_3$.

The second reduction of $Fe(FP)(ClO_4)$ is shown in Figure 6 C, the Soret band shifted from 418 to 428 nm upon the second reduction to form $Fe(FP)^-$. The shape and position of this band for $Fe(FP)^-$ was consistent with an RTIL nanodomain. Unfortunately, because $Fe(FP)^-$ in THF is mostly transparent in that spectral region, it is difficult to calculate the percent $Fe(FP)^-$ in the RTIL. A reasonable estimate can be made by comparing the ferric band in the starting spectra with the $Fe(FP)^-$ spectrum. In $AmNTf_2$, the two bands have nearly the same molar absorptivity, but in the mixed solution, the $Fe(FP)^-$ is 80 % of the ferric absorbance. This would indicate an enhanced solubility of $Fe(FP)^-$ in the RTIL nanodomain. The lack of good isosbectic points in the second reduction is consistent with the presence of some $Fe(FP)^-$ in the THF nanodomain.

The spectroelectrochemistry of Fe(FP)(Cl) in mixed solvents was more complex. The reduction of Fe(FP)(Cl) yields Fe(FP) in THF and $Fe(FP)(Cl)^-$ (initially) in $AmNTf_2$. As was shown in Figure 4 B, the $Fe(FP)(Cl)^-$ in $AmNTf_2$ slowly converted to Fe(FP) with a Soret band at 410 nm. In mixtures of THF/$AmNTf_2$, additional reactions are possible. Figure 7 shows the visible spectra of $Fe(FP)(Cl)^-$ in different mixtures. With no THF present, the Soret band for $Fe(FP)(Cl)^-$ at 435 nm is formed, which slowly converted to Fe(FP) (410 nm). In the presence of small amounts of THF (2 %), a new band at 418 nm appeared with a decrease in the 435 nm band. Eventually at 20 % THF, the $Fe(FP)(Cl)^-$ band is gone

with the 418 nm band being the most prominent. The band at 418 nm is indicative of the $Fe(FP)(THF)_2$ complex. The broadness of the band, though, indicates that there is significant partitioning between the THF and $AmNTf_2$ nanodomains. These results show a sharp transition in the coordination of the ferrous species with small amounts of THF. These spectral results are consistent with the strong curvature of the *E*° values versus %$AmNTf_2$ as the mixtures approach 100 %.

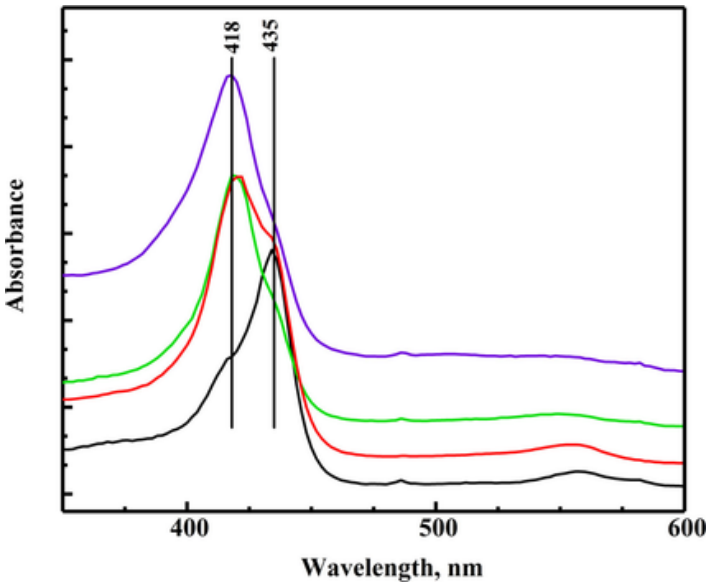

Figure 7 UV/Visible spectra of $Fe(FP)(Cl)^-$ in mixed $AmNTf_2$/THF solutions. 100 % $AmNTf_2$ (black), 98 % $AmNTf_2$ (red), 93 % $AmNTf_2$ (green), 50 % $AmNTf_2$ (blue).

^{19}F NMR of iron porphyrins in THF, $AmNTf_2$ and mixed solvent solutions

The ^{19}F NMR chemical shifts for the various iron porphyrin complexes in THF and $AmNTf_2$ are shown in Table 2. The values of the ferric and ferrous complexes in THF are consistent with previous reports, where available.[28, 29] One of the characteristics of the spectra is the splitting of the o- and m-resonances due to the asymmetry of the 5-coordinate complexes. The chemical shifts indicate that $Fe(FP)(THF)_2^+$ is the primary species of the $Fe(FP)(ClO_4)$ in THF. Interestingly, no splitting was observed for $Fe^{III}(FP)(ClO_4)$ in $AmNTf_2$ which would indicate that the perchlorate ligand is displaced in the RTIL. The lack of splitting is consistent with a bis-NTf_2^- complex, proposed earlier in this paper. Splitting of the *o*- and *m*-resonances was observed for Fe(FP)(Cl) in THF and $AmNTf_2$ (only m- and p-resonances were observed in $AmNTf_2$). Only minor shifts in the ferric species were observed when the RTIL solvent was replaced by THF, with maximum shifts of 1–2 ppm. This was consistent with the visible spectra.

Table 2. ^{19}F NMR spectra of iron porphyrin complexes

Compound	Solvent	*o*-Resonance	*p*-Resonance	*m*-Resonance	Reference
H_2FP	CD_2Cl_2	−137.1	−152.7	−162.1	[28a]
$Fe^{III}(FP)(ClO_4)$	THF	−134.7	−152.7	−161.7	this work
	$AmNTf_2$	−132.8	−151.3	−161.0	this work
$Fe^{III}(FP)Cl$	CD_2Cl_2	−102.0, −105.1	−148.5	−152.1, −157.0	[28a]
	[D_6]acetone	−105.8, −107.7	−150.2	−153.9, −156.0	[28b]
	THF	−118.1, −119.5	−153.1	−158.2, −160.5	this work
	[D_3]CH_3CN	−107.7, −108.8	−150.9	−154.7, −156.7	this work
	$AmNTf_2$	–	−149.0	−154.3, −156.5	this work
$Fe^{II}(FP)(THF)_2$	[D_8]THF	−140.4	−157.7	−165.3	[28a]
	THF	−141.8	−159.3	−167.1	this work
$Fe^{II}(FP)$	[D_8]toluene	−135.5	−152.2	−161.4	[28a]
	$AmNTf_2$	−129.9	−153.2 (−152.8)[a]	−160.6 (−160.1)[a]	this work
$Fe^{II}(FP)Cl^-$	[D_8]toluene	−131.0, −132.2	−157.9	−165.1, −166.0	[28a]
	[D_3]acetonitrile	−126.0, −127.7	−154.2	−160.3	[28c]
	[D_8]THF	−142.5	−163.4	−174.1	[28c]
$Fe(FP)^-$	THF	−141.5 (−141.5)	−162.1 (−162.3)	−172.9 (−173.0)	this work
	$AmNTf_2$	−137.0	−153.2	−160.6	this work

[a] Obtained by the reduction of Fe(FP)(Cl).

For the ferrous species, $Fe(FP)(ClO_4)$ and Fe(FP)(Cl) formed the same $Fe^{II}(FP)(THF)_2$ complex in THF (Table 2). No splitting in the *o*- or *m*-resonances were observed. While this does not prove that a $Fe^{II}(FP)(THF)_2$ complex was formed, the chemical shifts were different from the $Fe(FP)(Cl)^-$ complex in THF, made by the addition of a chloride salt. These results are consistent with the visible spectra, which were the same for both complexes. Larger shifts were observed though for $Fe^{II}(FP)$ when the solvent was changed from THF to $AmNTf_2$. The *o*-resonances decreased by about 11 ppm, while the *p*- and *m*-resonances decreased by 5–6 ppm. This also reflects changes in the visible spectra between the THF and $AmNTf_2$ environment. In addition, the $Fe^{II}(FP)$ spectra was the same in $AmNTf_2$ whether one started with the chloride or perchlorate complex. This was consistent with the slow dissociation of Cl^- from the $Fe^{II}(FP)(Cl)^-$ complex.

As with the ferrous complex, the $Fe(FP)^-$ complex was identical whether one started with the Cl^- or ClO_4^- complex. In THF, the *o*-resonance was quite similar to the ferrous complex, while the *p*-resonances increased by 4 ppm and the *m*-resonances by 11 ppm. In $AmNTf_2$, the chemical shifts of the *p*- and *m*-resonances decreased from their values in THF. In addition, in $AmNTf_2$, the *p*- and *m*-resonances for $Fe(FP)^-$ and $Fe^{II}(FP)$ are similar but the *o*-resonances differed.

In order to understand the solvation changes in mixed solvents, the ^{19}F NMR spectra for Fe(FP) complexes as a function of %$AmNTf_2$ were obtained. For the ferric complexes, the chemical shifts were small and the major effect of $AmNTf_2$ was a broadening due to the increase in viscosity. The ferrous porphyrins showed significant shifts when the solvent was changed. The *meta*-fluorine shifted from −167.1 to −161.8 ppm when the solvent was changed from THF to $AmNTf_2$. There were similar shifts for

the *para*-fluorine. The ^{19}F NMR spectra of THF/$AmNTf_2$ mixtures are shown in Figure 8 A. At lower concentrations of $AmNTf_2$ (less than 60–70 %), single ^{19}F NMR resonances were observed due to exchange between the $AmNTf_2$/THF nanodomains. This was different from the visible spectra where separate species were observed, due to the difference in the time domains for visible versus NMR spectroscopy. At higher concentrations of $AmNTf_2$, discrete resonances for the two nanodomains were observed. Figure 9 shows the deconvolution of Fe^{II}(FP) in 80 % $AmNTf_2$. The green shaded areas were identified as Fe^{II}(FP) in the $AmNTf_2$ nanodomain. The *meta*-resonances at −162.1/−163.1 ppm corresponded well with the −160.6 ppm value in pure $AmNTf_2$, with *para*-resonances at −155.3 ppm (−153.2 ppm in pure $AmNTf_2$) and *ortho*-resonances at −127.4 and −130.9 ppm, the average of which is close to the resonance in pure $AmNTf_2$ (−129.9 ppm). The split resonances may be due to the slow rotation of the phenyl groups in the highly viscous RTIL. The blue shaded resonances (−138.9, −155.8 and −164.2 ppm) corresponded well with $Fe^{II}(FP)(THF)_2$ (−141.8, −153.2 and −167.1 ppm). A minor red component was consistent with some residual ferric complex.

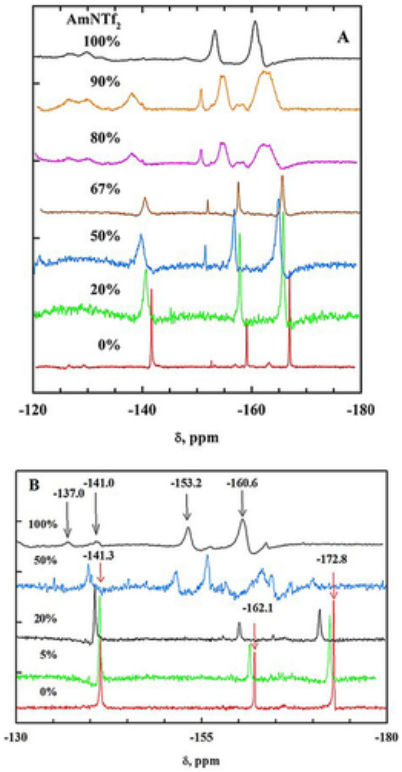

Figure 8 ^{19}F NMR of Fe^{II}(FP) (A) and $Fe(FP)^-$ (B) in mixed THF/$AmNTf_2$ solutions. (v/v)% $AmNTf_2$ are given in the figures.

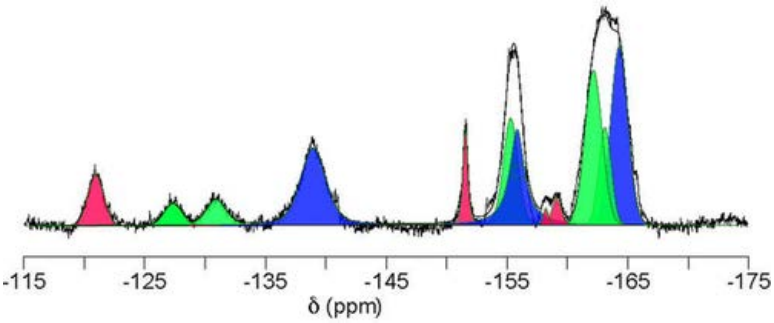

Figure 9 ^{19}F NMR spectrum of Fe(FP) in 80 % $AmNTf_2$/THF. Green peaks: Fe(FP) in $AmNTf_2$; Blue peaks: Fe(FP) in THF; Red peak: residual Fe(FP)(Cl).

The variation in the ^{19}F chemical shift of $Fe(FP)^-$ as a function of %RTIL is shown in Figure 8 B. Significant solvation within the RTIL nanodomain could be observed at low concentrations of $AmNTf_2$. This is to be expected as anions are better solvated within the RTIL than neutral species. Below 50 % $AmNTf_2$, single resonances were observed for each fluorine indicating fast exchange between the two nanodomains. At 50 % $AmNTf_2$, the resonances became broader, and resonances for the two domains began to appear. For example, the *meta*-resonances (−172.8 ppm in THF) shifted gradually to lower values up to 20 % $AmNTf_2$, a much weaker signal was seen in 50 % $AmNTf_2$ and the *meta*-resonance in $AmNTf_2$ (about −163 ppm) was the dominant species. The ^{19}F NMR spectra are consistent with significant solvation of the $Fe(FP)^-$ species in the RTIL-nanodomain around 50 % RTIL. This also corresponded to the beginning of the non-linearity in the $E°_2$ values versus %RTIL (or Gutmann AN). Dissolution in the RTIL appears to be correlated with the change in iron solvation from THF to NTf_2^-, as the %THF declined. This will be further investigated using EPR.

EPR spectra of $Fe(FP)^-$ in THF and $AmNTf_2$

Samples of $Fe(FP)^-$ were synthetized using borohydride reduction (which was also used for NMR analysis), and studied using EPR spectroscopy. The EPR spectra of $Fe(FP)^-$ in THF and $AmNTf_2$ are shown in Figure 10. The EPR spectrum of $Fe(FP)^-$ in THF (red trace) was consistent with the previous work of Srivatsa et al.[30] for $Fe(TPP)^-$ in DMF, with g-values of 2.29 and 1.93 (2.28 and 1.93 for $Fe(TPP)^-$). The $Fe(FP)^-$ complex has been characterized as a Fe^I complex with the unpaired electron in the d_{z2} orbital. The $g_\perp$ is quite sensitive to the axial coordination of the iron, with the $g_\perp$ decreasing in the presence of stronger ligands (e.g., pyridine).[30] When the solvent was changed to $AmNTf_2$, the $g_\perp$ value increased significantly to 2.65 (Figure 10, blue trace). This change reflects the loss of THF coordination, leaving an Fe^I species either uncoordinated or weakly coordinated with NTf_2^-. Donohoe et al.[31] speculated that the changes in the EPR in the presence of pyridine were due to the replacement of the solvent (DMF) with pyridine. This work is consistent with the observation that there is significant interaction between THF and Fe^I, at least at low temperatures.

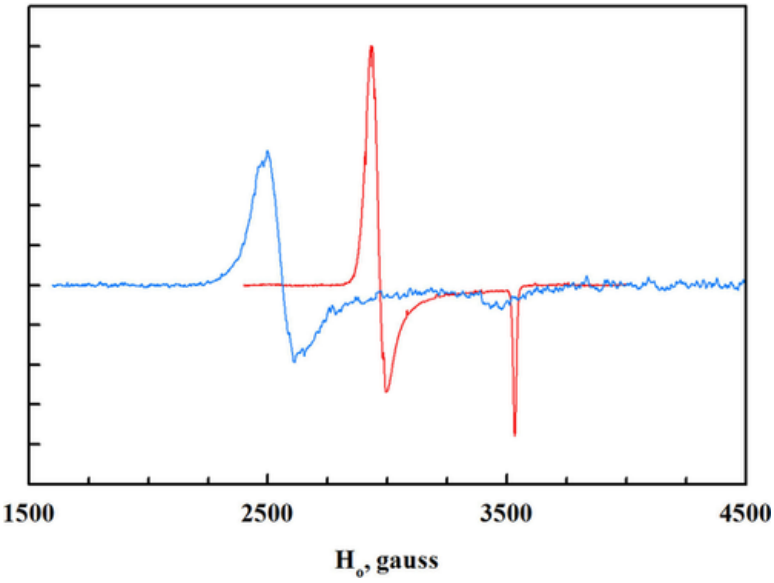

Figure 10 EPR spectra for $Fe(FP)^-$ in THF (red) and in $AmNTf_2$ (blue).

Solvation of iron porphyrins in mixed solvents and its effect on redox potentials

The effect of ionic liquids on the redox potentials is a combination of coordination changes and solvation of the iron complexes. The shifts in the $E°_1$ as a function of the Gutmann AN in the linear region (18 mV/AN) was similar to the Ni(OEP) oxidation (22 mV/AN), where the change in charge upon reduction was the same. The variation in $E°_1$ for Fe(FP)(Cl) was considerably larger (93 mV/AN) as compared to Ni(OEP) reduction (53 mV/AN). The large difference between $Fe(FP)(ClO_4)$ and Fe(FP)(Cl) is quite intriguing in that the porphyrin products are identical ($Fe^{II}(FP)(THF)_2$) and the interaction between the cation ($Fe^{III}(FP)(THF)_2^+$) or the neutral (Fe(FP)(Cl)) and an RTIL is minimal. The driving force for the shift in the $E°_1$ values for Fe(FP)(Cl), as the %RTIL is increased, is probably due to solvation of the Cl^- in the RTIL nanodomain. As a small anion, it should interact strongly with the RTIL.

As the %RTIL approaches 100 %, the ^{19}F NMR provides evidence for coordination changes as the source of the non-linearity in the $E°_1$ values as a function of log(%RTIL)/Gutmann AN. Even when the %RTIL was relatively high (80–90 %), coordination between the ferrous porphyrin and THF remained. The significant shifts in the $E°_1$ value versus %RTIL only occurred near 100 % RTIL, where coordination between the Fe^{II} porphyrin and THF was lost.

Generally, the visible spectra of reduction products in molecular solvents and RTILs are characterized by shifts in the absorbance maxima due to solvation effects. Overall the spectra in RTILs are similar to the spectra in molecular solvent. Examples of this are $Fe^{II}(FP)$ in this work, and $Ni(OEP)^-$.[2e] The exceptions to this observation though are quite enlightening. While the RTIL anions are generally very weak bases, they are still capable of displacing Cl^- from ferrous complexes.

The visible spectroelectrochemistry showed that $Fe^{II}(TP)$ in $AmNTf_2$ is coordinated, probably with the NTf_2^- anion. The ^{19}F NMR showed that the phenyl fluorine resonance were split as the %RTIL approached 100 %. At 100 % RTIL, single resonances were observed due to NTf_2^- coordination. The transfer between the THF and RTIL nanodomain can be written as [Eq. 9]:

$$Fe^{II}(FP)(THF)_2 + 2NTf_2^- \rightleftarrows Fe^{II}\,(NTf_2)_2^{2-} + 2THF \quad (9)$$

where $Fe^{II}(FP)(THF)_2$ is in the THF nanodomain and $Fe^{II}(FP)(NTf_2)_2^{2-}$ is in the RTIL nanodomain. At low %THF, this reaction would be expected to be slow. The charge on the product ferrous complex is probably minimized by strong ion pairing with the RTIL.

The spectral features of ferrous porphyrins are consistent with a six coordinate complex in $AmNTf_2$, even though coordination occurs with the NTf_2^- anion. This is possible due to the strong ion pairing of the RTIL to the anion. The displacement of anions such as Cl^- from the ferrous complex is slow, and is not seen on the voltammetric timescale. Entropy was probably the driving force for this reaction. As a result, the net stoichiometric reaction in voltammetry was a one-electron reduction of Fe(FP)(Cl) to $Fe(FP)(Cl)^-$ while, in spectroelectrochemistry or NMR spectroscopy, Fe(FP) was formed.

For the second reduction, the $E°_2$ for the Fe(FP)(Cl) and $Fe(FP)(ClO_4)$ as a function of Gutmann AN are nearly the same (56 and 55 mV/AN, respectively), using the initial linear region. This was quite similar to the $Ni(OEP)^{0/-1}$ redox process (53 mV/AN). As with the first reduction, the non-linear region of the $E°$ versus Gutmann AN correlated with the broadening and splitting of the ^{19}F NMR spectra. This was also probably due to coordination changes during the transfer of $Fe(FP)^-$ to the RTIL phase with loss of THF, which occurs at a lower %RTIL for the Fe^I porphyrin. The EPR showed a much weaker solvent interaction of $Fe(FP)^-$ with the RTIL, and was consistent with the loss of THF. A reaction similar to Reaction 9 can be written for $Fe(FP)^-$[Eq. 10]:

$$Fe(FP)(THF)^- \rightleftarrows FE(FP)^- + THF \quad (10)$$

in which $Fe(FP)(THF)^-$ is in the THF nanodomain and $Fe(FP)^-$ is in the RTIL nanodomain.

The most significant coordination changes between the molecular solvent and the RTIL complex is the $Fe(FP)^-$ complex. In THF, the visible spectrum for $Fe(FP)^-$ was considerably bleached due to delocalization of the d_{z2} electron to the porphyrin ring. On the other hand, $Fe(FP)^-$ in $AmNTf_2$ showed a metal centered reduction of Fe(FP) with a strong Soret band, quite similar to $Fe(TPP)^-$,[24c] as well as $Fe(FP)(Cl)^-$ in $AmNTf_2$. The mostly metal centered reduction is probably favored by the weaker interaction between the solvent anion (NTf_2^-) and the negatively charged $Fe(FP)^-$. Such a formulation was also consistent with the EPR spectrum where the shift in the *g*-value was related to a greater electron density on the d_{z2}-orbital. The opposite effect was observed for $Ni(OEPone)^-$, where the mostly metal centered reduction of $Ni(OEPone)^-$ in THF was switched to significant ring delocalization in $AmNTf_2$, as shown by the significant downshift in the ring carbonyl band.[2e]

Conclusion

This work shows that the solvent coordination of iron porphyrins in the presence of RTILs has a strong effect on the redox and spectroscopic properties. Previous work on mixed RTIL/molecular solvent solutions has shown a smooth transition in the redox potential as the solution was changed from pure molecular solvent to pure RTIL solutions. Iron porphyrins do not follow that behavior, with significant changes in the redox and visible spectra as the molecular solvent coordination is lost. Ni(OEP) shows only modest changes in the $E°$ versus %RTIL/Gutmann AN as the mixture approach pure RTIL. Similar behavior was observed for fullerides and dinitrobenzene. In the case of iron porphyrins, coordination with the molecular solvent (THF) maintains itself, even in RTIL-rich mixtures. Surprisingly, significant changes in the redox and visible spectra have been observed as the solvent system approaches neat RTIL. This behavior is more pronounced for the more negatively charged species, due to higher

partitioning within the RTIL nanodomains and the loss of solvent coordination. Therefore, while the linear relationship between the *E*° values and the Gutmann AN is a good measure of solvation changes, the non-linearity near 100 % is reflective of coordination changes at the metal site.

Changes in the electronic structure of the reduced product (metal vs. porphyrin reduction) should be reflected in the catalytic properties of the metal center. In addition to the positive shift in the redox potential by RTILs, the current work indicates that Fe^{I} porphyrins in an RTIL environment would be more nucleophilic, making them better catalysts for reactions that are initiated by nucleophilic attack. This finding is consistent with the recent work of Choi et al.,[7] where the iron porphyrin/RTIL system increased the rate and selectivity of CO_2 activation at very low over-potentials. In their work, the addition of an RTIL caused the overpotential for CO_2 reduction to be lowered by 670 mV, and a four-fold increase in the turnover frequency. Ongoing efforts in our laboratory are being extended towards studies on the effects of the RTIL nanodomains on the chemical reactivity of iron porphyrin redox systems.

Experimental Section

Chemicals

Ethyldimethylpropylammonium bis(trifluoromethylsulfonyl)imide ($AmNTf_2$), tetrabutylammonium borohydride ($TBABH_4$, 98 %), silver perchlorate ($AgClO_4$), iron tetrakis(pentafluorophenyl)porphyrin chloride ($FeF_{20}TPPCl$, 98 %), tetrabutylammonium perchlorate (TBAP) and anhydrous tetrahydrofuran (THF, 98.9 %) were purchased from Sigma-Aldrich Chemical Co. Decamethylferrocene (DmFc) (99%) was purchased from VWR. Anhydrous tetrahydrofuran (THF) was refluxed in the presence of sodium and benzophenone under nitrogen until the solution turned a persistent dark blue. Water was removed from the RTIL by passing N_2 over the solvent heated at 70–90 °C. The amount of water in the RTIL was measured by monitoring the stripping peak on a gold electrode due to water.[2d, 32] Substantial reduction in the water concentration was obtained as evidenced by the complete disappearance of the water stripping peak.

$Fe(TF_{20}PP)(ClO_4)$ ($Fe(FP)ClO_4$)) was prepared by exchanging the chloride ligand in $Fe(TF_{20}PP)Cl$ by using the procedure of Ogoshi et al.[33] Reduction of $Fe(TF_{20}PP)(ClO_4)$ was carried out by adding one equivalent of $TBABH_4$ in THF, and removing the solvent. Addition of 1.5 mole equivalent of $TBABH_4$ to the ferrous solution led to the low valent $Fe^{I}(FP)^{-}$.

Instrumentation

Cyclic voltammetry was carried out at a platinum electrode (1.6 mm or 10 μ), and a platinum wire was used as auxiliary electrode. Potentials were measured relative to the $Ag/AgNO_3$ (in CH_3CN) reference electrode. The measurements were carried out using a Model 600D Series Electrochemical Analyzer/Workstation (CHI Version 12.06). A low-volume thin layer quartz cell, which was purchased from BAS Instruments, was used for UV/Visible spectroelectrochemical experiments. A platinum mesh was used as working electrode, a platinum wire was used as auxiliary electrode. Potentials were measured relative to the $Ag/AgNO_3$ (in CH_3CN) reference electrode. UV/visible spectra were recorded on a HP8452A diode array spectrophotometer. All solutions were prepared and filled into the voltammetric or spectroelectrochemical cells in the glovebox under an argon environment. Proton and fluorine NMR measurements were performed using a Varian 400 MHz FT spectrometer. EPR measurements were performed at liquid nitrogen temperatures, using a Bruker ELEXSYS E600 equipped with an ER4415DM

cavity resonating at 9.63 GHz, an Oxford Instruments ITC503 temperature controller and ESR-900 He flow cryostat.

Procedures

For electrochemical experiments, all solutions were prepared and filled into cells in the glovebox under an argon environment. Tetrabutylammonium perchlorate was used as electrolyte in molecular solvent experiments. UV/Visible spectroelectrochemical experiments were carried out by either scanning or stepping the potentials at the corresponding waves. For mixture of molecular solvents/RTILs, a total volume of 0.3–0.5 mL for voltammetry, 0.2–0.5 mL NMR and 0.1–0.2 mL for spectroelectrochemistry were prepared using micropipette. The Gutmann acceptor numbers were calculated using an NMR procedure developed by Schmeisser et al.[34] and further described by Atifi and Ryan.[2e] The best fit empirical equation in Table S1 was generated using the curve fitter algorithm in MATLAB. Deconvolution of the ^{19}F NMR spectra was carried out using GRAM/32 AI software (ThermoGalactic).

Conflict of interest

The authors declare no conflict of interest.

Supporting Information

As a service to our authors and readers, this journal provides supporting information supplied by the authors. Such materials are peer reviewed and may be re-organized for online delivery, but are not copy-edited or typeset. Technical support issues arising from supporting information (other than missing files) should be addressed to the authors.

https://onlinelibrary.wiley.com/action/downloadSupplement?doi=10.1002%2Fchem.201701540&file=chem201701540-sup-0001-misc_information.pdf

References

1a P. Hapiot, C. Lagrost, *Chem. Rev.* 2008, 108, 2238–2264;
1b D. S. Silvester, R. G. Compton, *Z. Physik. Chem. (München, Germany)* 2006, 220, 1247–1274;
1c J. Zhang, A. M. Bond, *Analyst* 2005, 130, 1132–1147;
1d C. Chiappe, D. Pieraccini, *J. Phys. Org. Chem.* 2005, 18, 275–297.
2a M. Liang, X. X. Zhang, A. Kaintz, N. P. Ernsting, M. Maroncelli, *J. Phys. Chem. B* 2014, 118, 1340–1352;
2b J. N. Canongia Lopes, M. F. Costa Gomes, P. Husson, A. A. H. Pádua, L. P. Rebelo, S. Sarraute, M. Tariq, *J. Phys. Chem. B* 2011, 115, 6088–6099;
2c D. Zigah, A. Wang, C. Lagrost, P. Hapiot, *J. Phys. Chem. B* 2009, 113, 2019–2023;
2d A. Atifi, M. D. Ryan, *Anal. Chem.* 2014, 86, 6617–6625;
2e A. Atifi, M. D. Ryan, *Anal. Chem.* 2015, 87, 12245–12253;
2f A. Atifi, M. D. Ryan, *Electrochim. Acta* 2016, 191, 567–576.
3 M. Hammouche, D. Lexa, J. M. Saveant, M. Momenteau, *J. Electroanal. Chem.* 1988, 249, 347–351.
4 C. Costentin, S. Drouet, M. Robert, J. M. Savéant, *Science* 2012, 338, 90–94.
5a D. Quezada, J. Honores, M. Garcia, F. Armijo, M. Isaacs, *New J. Chem.* 2014, 38, 3606–3612;
5b J. Shen, M. J. Kolb, A. J. Göttle, M. T. M. Koper, *J. Phys. Chem. C* 2016, 120, 15714–15721.
6 B. A. Rosen, A. Salehi-Khojin, M. R. Thorson, W. Zhu, D. T. Whipple, P. J. A. Kenis, R. I. Masel, *Science* 2011, 334, 643–644.

7 J. Choi, T. M. Benedetti, R. Jalili, A. Walker, G. G. Wallace, D. L. Officer, *Chem. Eur. J.* 2016, 22, 14158–14161.
8 A. Katayama, T. Inomata, T. Ozawa, H. Masuda, *Electrochem. Commun.* 2016, 67, 6–10.
9a E. E. Switzer, R. Zeller, Q. Chen, K. Sieradzki, D. A. Buttry, C. Friesen, *J. Phys. Chem. C* 2013, 117, 8683–8690;
9b Y. T. Law, J. Schnaidt, S. Brimaud, R. J. Behm, *J. Power Sources* 2016, 333, 173–183.
10 X. Ji, D. S. Silvester, L. Aldous, C. Hardacre, R. G. Compton, *J. Phys. Chem. C* 2007, 111, 9562–9572.
11 G. P. S. Lau, M. Schreier, D. Vasilyev, R. Scopelliti, M. Grätzel, P. J. Dyson, *J. Am. Chem. Soc.* 2016, 138, 7820–7823.
12 Y. Oh, X. Hu, *Chem. Commun.* 2015, 51, 13698–13701.
13 L. Sun, G. K. Ramesha, P. V. Kamat, J. F. Brennecke, *Langmuir* 2014, 30, 6302–6308.
14a C. Costentin, S. Drouet, M. Robert, J. M. Savéant, *J. Am. Chem. Soc.* 2012, 134, 11235–11242;
14b C. Costentin, S. Drouet, G. Passard, M. Robert, J. M. Savéant, *J. Am. Chem. Soc.* 2013, 135, 9023–9031;
14c C. Costentin, G. Passard, M. Robert, J. M. Savéant, *J. Am. Chem. Soc.* 2014, 136, 11821–11829.
15D. R. Schreiber, M. C. De Lima, K. S. Pitzer, *J. Phys. Chem.* 1987, 91, 4087–4091.
16 A. A. H. Pádua, M. F. Costa Gomes, J. N. A. Canongia Lopes, *Acc. Chem. Res.* 2007, 40, 1087–1096.
17 A. J. Fry, *J. Electroanal. Chem.* 2003, 546, 35–39.
18a V. A. Nikitina, R. R. Nazmutdinov, G. A. Tsirlina, *J. Phys. Chem. B* 2011, 115, 668–677;
18b V. A. Nikitina, F. Gruber, M. Jansen, G. A. Tsirlina, *Electrochim. Acta* 2013, 103, 243–251.
19A. Hoshino, Y. Ohgo, M. Nakamura, *Inorg. Chem.* 2005, 44, 7333–7344.
20a I. Noviandri, K. N. Brown, D. S. Fleming, P. T. Gulyas, P. A. Lay, A. F. Masters, L. Phillips, *J. Phys. Chem. B* 1999, 103, 6713–6722;
20b A. A. J. Torriero, J. Sunarso, P. C. Howlett, *Electrochim. Acta* 2012, 82, 60–68;
20c J. Ruiz Aranzaes, M.-C. Daniel, D. Astruc, *Can. J. Chem.* 2006, 84, 288–299.
21 M. D. Ryan, C. DeSilva, *J. Porphyrins Phthalocyanines* 2007, 11, 519–523.
22a H. Kobayashi, Y. Yanagawa, *Bull. Chem. Soc. Jpn.* 1972, 45, 450–456;
22b C. A. Reed, T. Mashiko, W. R. Scheidt, K. Spartalian, G. Lang, *J. Am. Chem. Soc.* 1980, 102, 2302–2306.
23 A. Kütt, T. Rodima, J. Saame, E. Raamat, V. Mäemets, I. Kaljurand, I. A. Koppel, R. Y. Garlyauskayte, Y. L. Yagupolskii, L. M. Yagupolskii, E. Bernhardt, H. Willner, I. Leito, *J. Org. Chem.* 2011, 76, 391–395.
24a C. A. Reed, T. Mashiko, S. P. Bentley, M. E. Kastner, W. R. Scheidt, K. Spartalian, G. Lang, *J. Am. Chem. Soc.* 1979, 101, 2948–2958;
24b D. H. Dolphin, J. R. Sams, T. B. Tsin, *Inorg. Chem.* 1977, 16, 711–713;
24c C. A. Reed in Iron(I) and iron(IV) porphyrins, (Ed. K. M. Kadish), American Chemical Society, Washington, 1982, pp. 333–356;
24d D. Brault, M. Rougee, *Biochemistry* 1974, 13, 4598–4602;
24e I.-K. Choi, M. D. Ryan, *New J. Chem.* 1992, 16, 591–597;
24f C. De Silva, K. Czarnecki, M. D. Ryan, *Inorg. Chim. Acta* 1999, 287, 21–26.
25 D. Brault, M. Rougee, *Biochemistry* 1974, 13, 4591–4597.
26 K. M. Kadish, R. K. Rhodes, *Inorg. Chem.* 1983, 22, 1090–1094.
27 C. S. Consorti, P. A. Z. Suarez, R. F. de Souza, R. A. Burrow, D. H. Farrar, A. J. Lough, W. Loh, L. H. M. Da Silva, J. Dupont, *J. Phys. Chem. B* 2005, 109, 4341–4349.

28a B. Song, K. Park, B. Yu, *J. Korean Chem. Soc.* 1997, 41, 495–501;
28b E. R. Birnbaum, J. A. Hedge, M. W. Grinstaff, W. P. Schaefer, L. Henling, J. A. Labinger, J. E. Bercaw, H. B. Gray, *Inorg. Chem.* 1995, 34, 3625–3632;
28c B. H. Song, B. Park, C. H. Han, *Bull. Korean Chem. Soc.* 2002, 23, 119–122.
29 B. Song, B.-S. Yu, *Bull. Korean Chem. Soc.* 2003, 24, 981–985.
30 G. S. Srivatsa, D. T. Sawyer, N. J. Boldt, D. F. Bocian, *Inorg. Chem.* 1985, 24, 2123–2125.
31 R. J. Donohoe, M. Atamian, D. F. Bocian, *J. Am. Chem. Soc.* 1987, 109, 5593–5599.
32 C. Zhao, A. M. Bond, X. Lu, *Anal. Chem.* 2012, 84, 2784–2791.
33 H. Ogoshi, E. Watanabe, Z. Yoshida, *Chem. Lett.* 1973, 2, 989–992.
34 M. Schmeisser, P. Illner, R. Puchta, A. Zahl, R. van Eldik, *Chem. Eur. J.* 2012, 18, 10969–10982.